Optics and Lasers in Engineering 78 (2016) 1–7

Contents lists available at ScienceDirect

Optics and Lasers in Engineering

journal homepage: www.elsevier.com/locate/optlaseng

Design and fabrication of an angle-scanning based platform for the construction of surface plasmon resonance biosensor

Jiandong Hu [a,b,*], Baiqiong Cao [a], Shun Wang [c], Jianwei Li [a], Wensong Wei [a], Yuanyuan Zhao [d], Xinran Hu [e], Juanhua Zhu [a], Min Jiang [f], Xiaohui Sun [a], Ruipeng Chen [a], Liuzheng Ma [a]

[a] Department of Electrical Engineering, Henan Agricultural University, Zhengzhou 450002, China
[b] State Key Laboratory of Wheat and Maize Crop Science, Zhengzhou 450002, China
[c] Henan Nongda Xunjie Measurement and Technology Co. Ltd., Zhengzhou 450002, China
[d] Hanan Mechanical and Electrical Vocational College, Zhenzhou 451191, China
[e] School of Human Nutrition and Dietetics, McGill University, Macdonald Campus 21, 111 Lakeshore Road, Ste Anne de Bellevue, Quebec, Canada H9X 3V9
[f] College of life sciences, Henan Agricultural University, Zhengzhou 450002, China

ARTICLE INFO

Article history:
Received 20 February 2015
Received in revised form
7 September 2015
Accepted 8 September 2015
Available online 23 October 2015

Keywords:
Optic SPR biosensing platform
Laser line generator
Angle-scanning
An area CCD array

ABSTRACT

A sensing system for an angle-scanning optical surface-plasmon-resonance (SPR) based biosensor has been designed with a laser line generator in which a P polarizer is embedded to utilize as an excitation source for producing the surface plasmon wave. In this system, the emitting beam from the laser line generator is controlled to realize the angle-scanning using a variable speed direct current (DC) motor. The light beam reflected from the prism deposited with a 50 nm Au film is then captured using the area CCD array which was controlled by a personal computer (PC) via a universal serial bus (USB) interface. The photoelectric signals from the high speed digital camera (an area CCD array) were converted by a 16 bit A/D converter before it transferred to the PC. One of the advantages of this SPR biosensing platform is greatly demonstrated by the label-free and real-time bio-molecular analysis without moving the area CCD array by following the laser line generator. It also could provide a low-cost surface plasmon resonance platform to improve the detection range in the measurement of bioanalytes. The SPR curve displayed on the PC screen promptly is formed by the effective data from the image on the area CCD array and the sensing responses of the platform to bulk refractive indices were calibrated using various concentrations of ethanol solution. These ethanol concentrations indicated with volumetric fraction of 5%, 10%, 15%, 20%, and 25%, respectively, were experimented to validate the performance of the angle-scanning optic SPR biosensing platform. As a result, the SPR sensor was capable to detect a change in the refractive index of the ethanol solution with the relative high linearity at the correlation coefficient of 0.9842. This greatly enhanced detection range is obtained from the position relationship between the laser line generator and the right-angle prism to allow direct quantification of the samples over a wide range of concentrations.

1. Introduction

In recent years, the optic surface-plasmon-resonance (SPR) biosensor has been developed rapidly with the cutting-edge features of label-free biomolecular interactions, such as protein–protein, protein-DNA, drug-target, antigen–antibody binding, that provides information on kinetic analysis (association and dissociation process), binding affinity, concentration analysis and real-time molecule detection [1–4]. In principle, SPR is highly sensitive to the variations of refractive index near to the Au film surface or the mass of substances attached on it [5]. The SPR biosensor can detect the binding of biochemical molecules with a high sensitivity in real-time [6–9]. Therefore, it is widely exploited in agriculture, food safety, drug screening, medical diagnostics and environmental monitoring fields [10]. In contrast, traditional analysis methods including the X-ray photo-electronic spectroscopy (XPS) [11], Auger electronic spectroscopy (AES) [12], Secondary-ion mass spectrometry (SIMS) [13], Gas Chromatography (GC) [14], High Performance Liquid Chromatography (HPLC), Gas Chromatography–Mass Spectrometry (GC–MS) and Liquid Chromatography–Mass Spectrometry (LC–MS) cannot be used to study the biomolecular kinetic process [15,16]. Furthermore,

* Corresponding author at: Department of Electrical Engineering, Henan Agricultural University, Zhengzhou 450002, China.
E-mail address: jiandonghu@163.com (J. Hu).

http://dx.doi.org/10.1016/j.optlaseng.2015.09.004
0143-8166/

the instruments designed on principles of the spectroscopy technology are expensive, and the complicated preparation of samples and professional persons were needed in operations to detect the bioanalytes qualitatively and quantitatively. However, the SPR biosensor is not only able to monitor the kinetic process of biomolecular interactions in real-time, but also to detect the target samples at lower level concentrations under a small sample volume [17]. In the detection of DNA hybridization, the small DNA fragments can be also detected at the label free situation by using the SPR biosensor, such as 54 fM (femtomole, fM) [18]. Several hours or days were needed to complete the analysis of kinetic process of biomolecular interaction by using the traditional method for biochemical analysis, while only a few minutes are consumed to obtain the results of biomolecular interaction by using the optical SPR biosensor [19]. Quartz crystal microbalance (QCM) was utilized to monitor the kinetic process of proteins and biomolecular adsorption in real-time, although the QCM responses occur at a later time than the SPR responses [20]. A novel multi-channel fiber optic SPR sensor has been constructed to perform the analysis of biomolecular interactions [21]. Currently, the application requirements of an optical SPR bio-analyzer used in environmental monitoring, agriculture and medicine have become a very urgent requirement [22,23]. Many academic and engineering efforts have been aimed at the miniaturization of the biosensor system, such as the portable bio-analyzer with high-throughput, non-destructive, low cost and label free features applied in environmental monitoring, safety monitoring for foods, and the product quality control. Several groups have developed the miniaturized SPR bio-analyzers to reach the demands for using in the bio-analytical field [24–26]. A compact system based on SPR prism sensor using laser line generator has been preliminarily designed [27]. Nevertheless, the requirement for low cost SPR bio-analyzers with a high stability and the simultaneous analysis of multiple analytes on-site is steadily increasing.

In this work, we report a low cost SPR sensing scheme with the angle-scanning optic SPR biosensing platform using a laser line generator. The beam from the laser line generator is controlled to scan the Au film to realize the angle-scanning using a variable speed DC motor. The reflected light from the prism was then captured by a digital camera (an area CCD array) which was fixed on the supporting frame. It provides a low cost SPR biosensing platform that greatly facilitates the label-free and real-time biomolecular analysis. To greatly improve the detection efficiency of the SPR bio-analyzer, the area CCD array working at a high flame rate in excess of 15 frames per second is used to collect the SPR response signals produced by the reflected beam on the CCD array. Compared with the linear CCD array, the area CCD array can broaden the region of interesting (ROF) and provide a fundamental principle for realizing multiple channels to detect the sample solutions. In conventional SPR systems, the CCD array was moved by following the light source. Especially, the use of refractive index matching oils in the optical coupling process was inevitable. In this SPR biosensing platform, a 50 nm Au film was deposited on the small prism, which can be replaced conveniently when the Au film was scrapped after using over times. Thus this procedure for performing the optical coupling with matching oil is obviated.

2. Materials and methods

2.1. Materials

The laser line generator (dimension ϕ16 mm × 45 mm (L), wavelength 780 nm, beam divergent angle 65°) was purchased from SFOLT Co. Ltd. (Shanghai, China). The digital camera (an area CCD image sensor) was purchased from China Daheng Co., Ltd. The high speed acquisition circuit board was purchased from Tianjin Brilliance Photoelectric Technology Co., Ltd. (Tianjin, China). BK7 prism with 50 nm Au film was customized in Changchun Dingxin photoelectric Co. Ltd. (Changchun, China). The optical adjustment clamp for holding the right angle prism was fabricated in Henan Nongda Xuejie Measurement and Testing Technology Co., Ltd. (Zhengzhou, China). Ethanol and 1 mol/L phosphate buffered saline (PBS) buffer (pH7.4) were purchased from Shanghai General Chemical Reagent Factory (Shanghai, China).

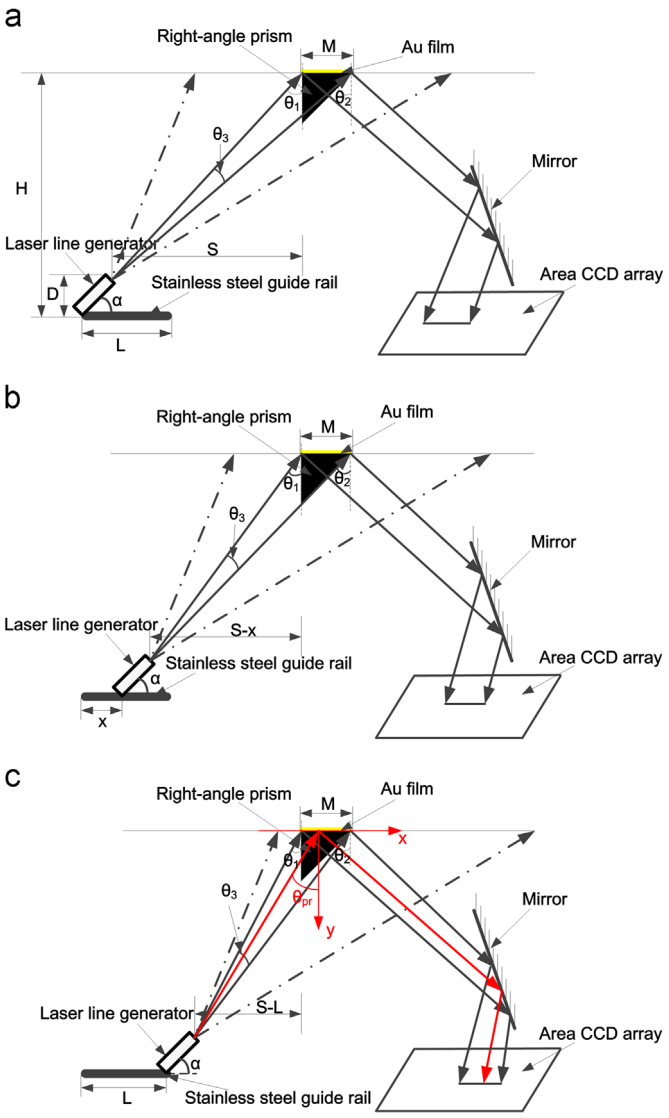

Fig. 1. Schematic of angle-scanning based SPR biosensor using a laser line generator; a. The laser line generator was located at the left side of the stainless steel guide rail, b. The laser line generator was located at the position x away from the left side, while c indicated the right side position.

2.2. The fundamental principle of the SPR biosensor

The schematic diagram of this SPR biosensing platform designed by using a laser line generator with angle-scanning is shown in Fig. 1. The laser line generator combining with angle-scanning system was utilized to change the incident angle to excite the SPR wave occurred at the interface between the Au film deposited on the prism and dielectric adjacent to the Au film to produce the SPR phenomenon. A DC motor working at variable speeds was used to keep the laser line generator moving back and forth along the stainless steel guide rail. Although the laser beam from the laser line generator was scanned gradually on the Au film

at the same divergent angle, the photoelectric signals from the area CCD array were obtained to establish the SPR curve only at the forward direction from the initial position, while nothing being recorded on the way that the laser line generator returns back to the initial position. The speed of the DC motor controlled by the PC on the way back is faster than the speed on the forward way. Before a sample solution was flown through the surface of the Au film, an initial angle should be estimated prior to the occurrence of total internal reflection at the interface between the prism and Au film. Thereafter, the SPR phenomenon was produced at a certain incident angle over the critical angle of total internal reflection.

From Fig. 1, Fig. 1a and c are shown that the laser liner generator controlled by the DC motor was located at the right side and the left side of the stainless steel guide rail, respectively. From Fig. 1c, it is known that the evanescent wave produced from the total internal reflection acts on the prism can excite a standing charge density wave on the gold surface [28]. A surface plasmon wave will be produced by the standing charge density at the interface between the metal film and the biological medium. The surface plasmon wave is a P-polarized electromagnetic wave due to a P-polarized light being parallel to the incident plane, while the S-polarized light being perpendicular to the incident plane.

For the SPR biosensor constructed by a prism with the coupling method of the attenuated total reflection, the propagation constants of the incident light wave and the surface plasmon wave along the x axis will be obtained in Eq. (1) and Eq. (2).

$$k_x^{pr} = \sqrt{\varepsilon_{pr}}\frac{\omega}{c}\ \sin\ \theta_{pr} \tag{1}$$

$$k_x^{sp} = \sqrt{\frac{\varepsilon_m^{\sim} \varepsilon_s}{\varepsilon_m^{\sim} + \varepsilon_s}}\frac{\omega}{c} \tag{2}$$

$$k_x^{pr} = \sqrt{\varepsilon_{pr}}\frac{\omega}{c}\ \sin\ \theta_{pr} = \sqrt{\frac{\varepsilon_m^{\sim} \varepsilon_s}{\varepsilon_m^{\sim} + \varepsilon_s}}\frac{\omega}{c} = k_x^{sp} \tag{3}$$

where the propagation constants for incident light wave and the surface plasmon wave are indicated with k_x^{sp} and k_x^{pr}, respectively. ε_{pr} is the refractive index of the prism, while $\varepsilon\sim_m$ is the complex refractive index of the metal film. θ_{pr} is the angle formed between the incident light and the normal line of the prism. ε_s is the refractive index of the biological sample flowed through the Au film surface. C is the speed of light and omega ω is the frequency of the surface plasmon wave.

Both propagation constants will be equal, $k_x^{sp} = k_x^{pr} = k_x$ while the surface plasmon resonance phenomenon occurring. At the resonance point, the intensity of the incident light is absorbed greatly, while the intensity of reflective light is approximately zero. By using this relationship, the refractive index of the biological sample bound on the surface of the Au film will be calculated. After the light at a certain wavelength and a certain angle is shone on the interface between the prism and the Au film, the surface plasmon and the photon inside the Au film will be absorbed. This is seen by a minimum intensity value in the reflection spectra. The position of the minima is indicative of the chemistry on the Au film surface of the SPR sensor. The shift for the minimum value is a measure of the dielectric constant or refractive index changed on the Au surface.

In this experiment, the laser line generator consisting of a P polarizer was customized in SFOLT Co. Ltd. The black dash-dotted line denoted the laser beam at a certain divergent angle, and the black solid line is the effective light beam irradiated on the surface of Au film to produce the SPR phenomenon after a sample solution was flowed through the Au film. Due to the small size of the Au film (6 mm × 3 mm), the irradiation range of the laser beam used in our experiments can completely cover the surface of Au film. The reflected light beam from the prism was first reflected by a mirror and then recorded by the area CCD array, which was connected with an acquisition circuit. The photoelectric signals were then transferred to the PC for the further analysis.

From Fig. 1, the angle α between the laser line generator and the stainless steel guide rail and the height D between the front-end of the laser line generator and the stainless steel guide rail sensitively affect the effective incident angle which the free electrons inside the Au film are excited to produce the SPR phenomenon. In order to obtain the relationship between the incident angle α and the position of the laser line generator (denoted with D) approximately, θ_1, θ_2 and θ_3 are calculated from the Eqs. (4) and (5). θ_1 and θ_2 are the angles between the laser rays (shown in black solid line) and the froth-end and back-end of the Au film, respectively, while θ_3 is the angle between the two laser rays indicated with the black solid line (see Fig. 1).

$$\begin{cases} \tan\ \theta_1 = \frac{S}{H-D} \\ \tan\ \theta_2 = \frac{S+M}{H-D} \\ \theta_3 = \theta_2 - \theta_1 \end{cases} \tag{4}$$

$$\begin{cases} \tan\ \theta_1 = \frac{S-L}{H-D} \\ \tan\ \theta_2 = \frac{S-L+M}{H-D} \\ \theta_3 = \theta_2 - \theta_1 \end{cases} \tag{5}$$

where L denotes the single-way distance for the laser line generator moving from left to right (L, less than 25 mm); H denotes the distance between the stainless steel guide rail and Au film; S denotes the horizontal distance between the central point of the front-end of the laser line generator and the front-end of Au film, and M denotes the length of the Au film. Provided that the laser line generator is moved from the leftmost position x (shown in Fig. 1), θ_3 can be calculated from the Eq. (6).

$$\theta_3 = \left[\arctan\left(\frac{S-X+M}{H-D}\right)\right] - \left[\arctan\left(\frac{S-X}{H-D}\right)\right] \tag{6}$$

As can be seen from the Eq. (6), the changes of the angle θ_3 is related to the reciprocating motion (denotes with x) of the laser liner generator. The relationship determined by the Eq. (6) showed that the incident angle θ_3 plays a crucial role in the design of the platform of this SPR biosensor.

Fig. 1b shows that the position indicated with the incident angle θ_3 to the surface of the Au film will be changed with the changing position x. The relationship indicated with the incident angle θ_3 is used to evaluate the dynamic detection range of this SPR biosensing platform.

2.3. Design of this experimental platform

The schematic diagram of the platform of an angle-scanning based optic SPR biosensor using a laser line generator was shown in Fig. 2.

This platform consists of a laser line generator, area CCD array, optical adjustment clamp, acquisition circuit board, a right-angle prism deposited with 50 nm Au film, an optical P polarizer, and the flow cell with the dimension of 3.5 mm (L) × 0.5 mm (W) × 0.25 mm (H) [29]. VC++ program was developed to complete the SPR response signals acquisition, to analyze the data stored in PC and to display the SPR curves on the screen. The area CCD array does not need to be moved with the laser line generator. A semi-sphere prism maybe used to continuously excite the SPR phenomena. However, it is not conductive to mount the laser line generator. After preliminary experiments, the right-angle prism was found to meet the requirements easily because the incident angle θ_3 obtained from the right-angle prism is larger than the angle from the equilateral-triangle prism (see Fig. 3). For the right-

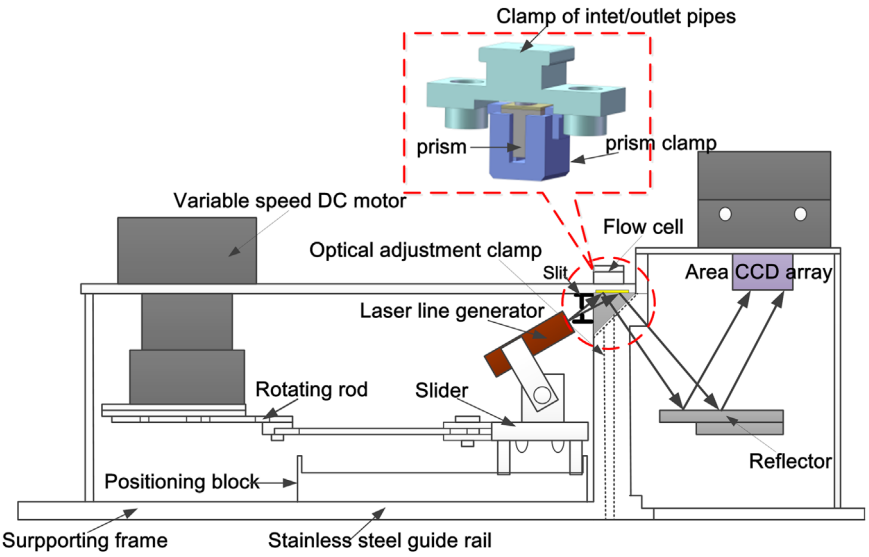

Fig. 2. Structure diagram of the angle-scanning based optical surface plasmon resonance biosensor using the laser line generator.

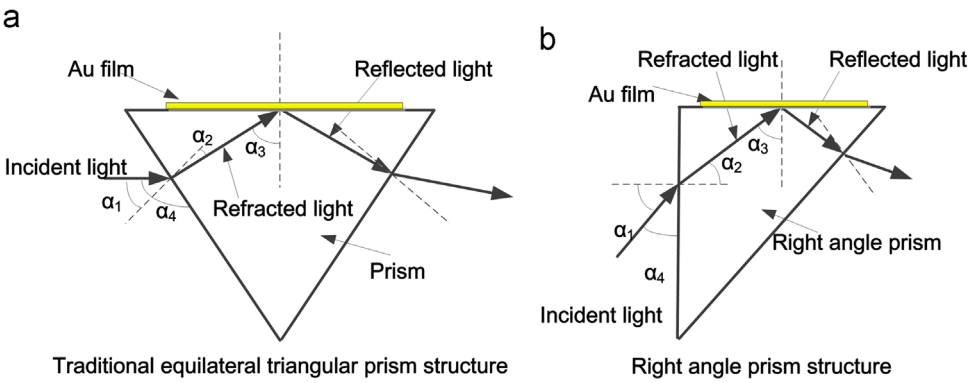

Fig. 3. Schematic diagram of incident and reflection of the laser beams for the equilateral triangular prism and the right angle prism.

angle prism, one rectangular surface is deposited with a layer of approximately 50 nm Au film. The laser beam providing a certain angle shines on the surface of the right-angle side of the prism. Therefore, a bunch of straight beam impinges on the surface of the Au film at the right-angle side. By calculation, the attenuated total reflection was occurred at the end of the right-angle prism by adjusting the effective incident angle θ_3.

Schematic diagrams for the comparison of the laser beams through the equilateral-triangle prism and right-angle prism are depicted in Fig. 3.

As shown in Fig. 3, α_3 can be calculated by the triangle formula from α_2, and the incident angle α_1 can also be calculated from the Snell's law. For example, take the consideration of the SPR angle obtained from the deionized water through the flow cell, the SPR angle around 72° is validated from this setup (the index of refraction of deionized water is 1.334. The index of refraction of the prism is 1.5138 (BK7 glass), while the index of refraction of air is 1). Therefore, the incident angles α_1, α_4 are calculated to be approximately 18° and 108°, respectively, if the traditional equilateral-triangular prism was used (Fig. 3a). The SPR angle ranged from 62° to 82° are obtained generally from this setup when the deionized water was flowed through the Au film. The angle α_4 will be gradually increased (larger than 72°) with the increment of SPR angle obtained from the sample solution, which is greater than the SPR angle (72°) from the deionized water. Consequently, the incident angle α_1 resulted from the laser line generator beam is also magnified. The laser beam produced by the laser line generator at the divergent angle of 65° cannot reach the prism due to the narrow space between the laser line generator and the prism. For solving this problem resulted from the special configuration of light source, the right-angle prism was chosen in this experiment (Fig. 3b). For this right-angle prism, provided the SPR angle of 72° is also obtained from the deionized water, the incident angles α_1 and α_4 were calculated to be 23° and 67° from the Snell formula. The angle α_4 can be approached to 90° with increasing of the SPR angle. Consequently, the incident angle α_1 reaches to zero, approximately. This consideration is to avoid the interference caused by the reflected light perfectly.

After the reflected light impinges onto the area CCD array, the SPR curves can be established from the photoelectric signals corresponding to different reflected angles, which were converted by the area CCD array. Prior to this experiment, the structural parameters illustrated in Fig. 1, including *L, H, S, M,* and *D*, are set. Therefore, the initial conditions can be adjusted easily according to the different measurement requirements to improve the dynamic detection range of the SPR biosensing platform using the laser line generator.

3. Results and analysis

For this CCD camera, the images formed by the SPR responses were recorded on the CCD for the ethanol concentrations ranged from 0% to 25% (see Fig. 4). From Fig. 4, the resonance position was

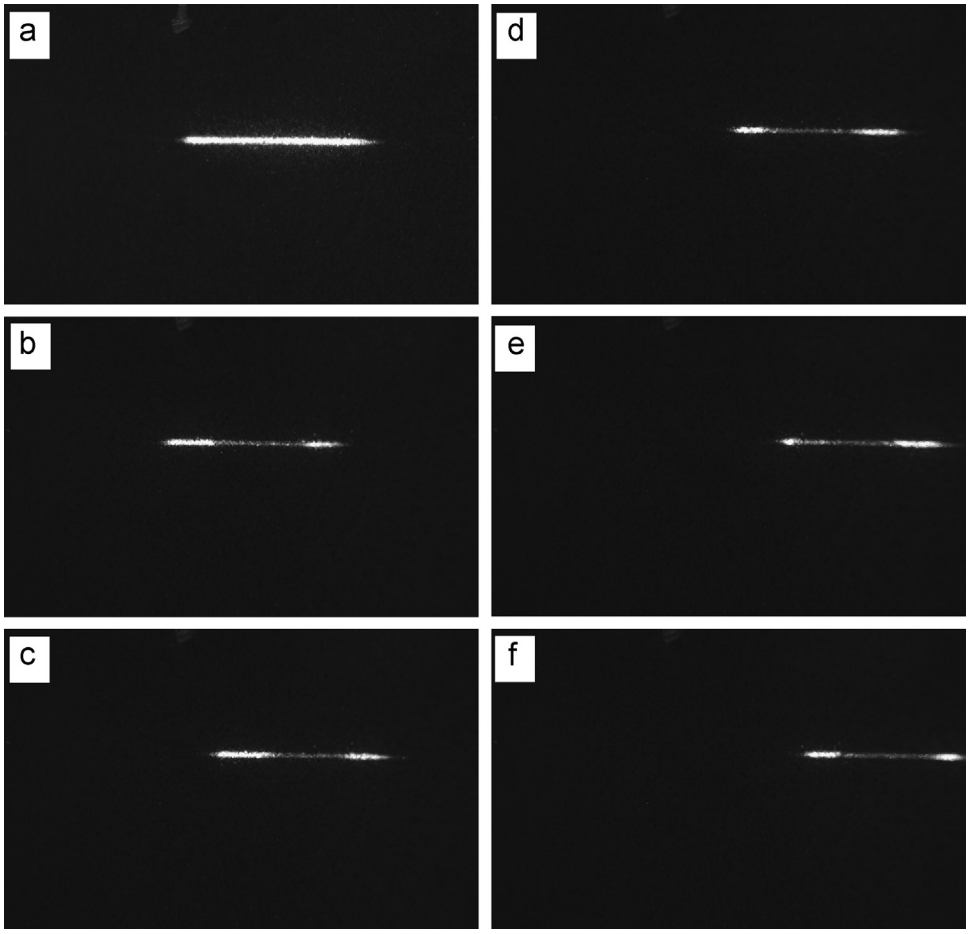

Fig. 4. The images recorded on the area CCD area for the ethanol concentrations ranged from 0% to 25% in volumetric factors. a. 0%, b. 5%, c. 10%, d. 15%, e. 20%, and f. 25%.

shifted to the right obviously. The images obtained from the SPR biosensing platform using the laser line generator are stored in a 3-dimensional value.

A number of 2D images are precisely taken by the area CCD array while the laser line generator is moving on the forward way. Then each 2D image is averaged in one dimension resulting in the 1D data. Finally, a number of 1D data is averaged to achieve a single 1D data. The response units can be derived from the single 1D data by performing the calibration. The SPR response curve was obtained by processing these image data obtained from the different concentrations of ethanol solution that flowed through the flow cell attached on the surface of the Au film of the SPR biosensor. Provided that N images were collected at certain sampling rate from the area CCD array, the procedures for the data processing of images can be described as follows: (1) convert the 3-dimensional image data into a 2-dimensional image data by accumulating all gray values along Y coordinate at the same X coordinate. Then the 2-dimensional data set was formed with the new X and Y coordinate. (2) Process the data with mean filtering. The gray level is described as:

$$\{g[i,j],\ i=1,2,\ldots,n;\ j=1,2,\ldots,m\} \tag{7}$$

The gray level related to the photoelectric signal from the CCD array is $g_{11}, g_{12}, g_{13}, \ldots, g_{1n}$ at $i=1$. For a set of measured data, a window size included of Matrix $M \times N$ is produced in the upper PC. The average value of gray level at $i=1$ corresponding to X_1 is given by:

$$Y[1]=\frac{1}{N}\sum_{j=1}^{N} g(1,j) \tag{8}$$

Then moving on the next data subset $i=2$, the sampling values are also expressed as $g_{21}, g_{22}, g_{23}, \ldots, g_{2n}$, and the average value of this new data set at $i=2$ corresponding to X_2 is given by:

$$Y[2]=\frac{1}{N}\sum_{j=1}^{N} g(2,j) \tag{9}$$

and so on. The new data set obtained was

$$\{[x(i),y(j)],\ i=1,2,3,\ldots,m;\ j=1,2,3,\ldots,n\} \tag{10}$$

In this experiment, the DC motor drives the laser line generator to do reciprocating motion at a variable speed and the area CCD array periodically collects the reflected signals. For the laser line generator beam scanning the Au film surface, the closer the laser line generator to the Au film, the smaller the effective incident angle is. The SPR phenomenon occurred at a certain position of the laser line generator. Generally, the data from the area CCD array can be a relatively highly consistence as long as the acquisition time of the area CCD array is integer times of its period of the reciprocating motion. However, it is not always working at integral times of its period, so the acquisition rate of the area CCD array is a parameter worth of considering. In this experiment, the area CCD array acquisition rate is 15 fps (frame per second), while the laser line generator moves at the rate of 5 mm/s to ensure the area CCD array can capture a clear image and record all trajectories. 120, 135,

150 images were taken from the known concentration of 10% ethanol solution in volumetric faction under this experiment, respectively. The results have a great consistency obtained by accumulating them and the correlation coefficient of 0.9972 was obtained. Although the acquisition time does not need to be strictly limited, the acquisition rate plays a crucial role during the process of measurement to obtain the adequate data. The performance can be improved greatly if the complete image of the SPR phenomenon could be obtained under the correlation coefficient being over 0.98 experimentally. The intensity of response signals (response unit, *RU*) is calculated with the same method as in the previously reported works [30]. In this experiment, the 25 images were captured during one cycle and totally 4 cycles are needed for obtaining the optimized SPR curve.

The sensing response of the SPR biosensor platform to the bulk refractive index was calibrated using various concentrations of ethanol solution to validate the performance of this SPR biosensing platform. In processing the image projected on the area CCD array, it is not easy to obtain the response position on the CCD directly due to the wide region of interesting from this SPR biosensing platform. Therefore, a centroid algorithm was chosen to get the resonance position on the CCD. Taking the SPR response curve obtained from the known concentration of ethanol solution as an example, the delta response unit (ΔRU) can be calculated by subtracting the RUs from the PBS flowed through the flow cell with the RUs obtained from the ethanol solution over Au film surface of the biosensor. The sensorgram of a sensing response at the concentration of ethanol solution of 5%, 10%, 15%, 20% and 25% in volumetric factions was shown in Fig. 5.

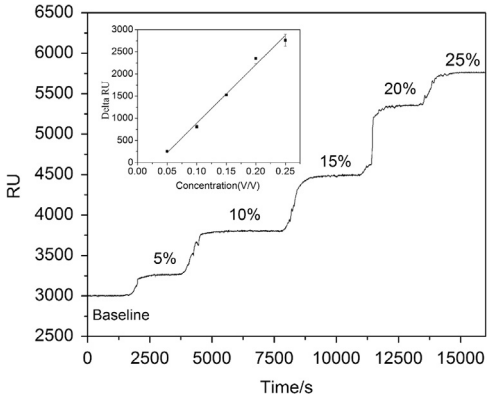

Fig. 5. Sensorgram of a sensing response with inset response signals at the concentrations of ethanol solution of 5%, 10%, 15%, 20% and 25% in volumetric factions. The report points set during these experiments are denoted by baseline, 5%, 10%, 15%, 20% and 25%. Baseline refers to the report points set 4 min before the injection of the ethanol solutions. It is defined as baseline. 5%, 10%, 15%, 20% and 25% refer to the report points after injection of ethanol solutions from 5% to 25% in volumetric factions, accordingly. The inset at the upper left is a relationship curve established between different concentration of ethanol solutions and ΔRU value.

From the inset in Fig. 5, the sensitivity of the SPR biosensor can be expressed with the measured concentration of ethanol solutions related to the ΔRU values, which clearly reflects the excellent performance of the SPR biosensing platform. The time for a single angular scan depends on the kinetic constants calculated from the interactions between two bio-molecules on the Au film. It can be adjusted by changing the speed of the DC motor to reach an optimized value. For this SPR platform, only 8 s being required for the single angular scan in one way and 5 min for the interaction to reach an equilibrium point for the ethanol solutions.

As can be seen from the RUs produced from the angle-scanning based SPR biosensor using the laser line generator, the RUs corresponding to the bulk index of refraction of the ethanol solutions and an excellent linear relationship between them can be easily obtained by the linear fitting algorithm with the equation of $y = 2636.74x - 877.1312$ at the correlation coefficient of 0.9842. The calculated sensitivity of this biosensor is 845.60 RU/Volumetric fractions of the ethanol solutions. The specifications comparison between this SPR platform and those standard SPR setup is shown in Table 1. From Table 1, it provides comparability among the similar commercial products on technical parameters.

4. Conclusions

In summary, a SPR biosensing platform was developed by using the laser line generator via the modulation of the beam divergent angle with the variable speed DC motor controlled by the PC automatically. The single-way distance (indicated with *L* in Fig. 1) for the laser line generator moving from left to right is less than 25 mm. A more compact portable SPR platform can be achieved successfully. The current SPR biosensing platform was designed to be low cost and wide dynamic detection range for the on-site kinetic analysis of bio-molecular interactions. The detection efficiency and sample analysis speed were greatly improved due to the elimination of manual operations. The right-angle prism instead of equilateral-triangular prism has utilized to reduce the influence of incident light which is always used to excite the surface plasmon inside the Au film. The different concentrations of ethanol solution in volumetric fractions have designed to validate the performance of this angle-scanning optic SPR biosensing platform. The mean filtering algorithm has been applied to process the image data occurred in the range of interesting. Correspondingly, an order modified centroid algorithm with a dynamic

Table 1
A comparison with similar products.

Technical parameters	Specifications		
Bioanalyzer	Biacore3000	AUTOLAB Esprit	This SPR platform using a laser line generator
No. of channels	4	2	1
Sample volume	0.02 μl	20–150 μl	200–400 μl
Autosampler	Full automatic operation	Full automatic, Semi-automatic, Manually operation	Peristaltic pump
Baseline noise	–	0.1 mº	< 5 RU (within 2 h)
Fixed wavelength	–	670 nm	780 nm
Weight	–	40 kg	Less than 10 kg
Angle-scanning range	–	–	Large than 30°
Concentration range	10^{-3}–10^{-11} M	$10^{-3} \times 10^{-10}$ M	–
Refractive index range	1.33–1.40	1.26–1.38 (BK7 slider) 1.32–1.44 (N-BAF3 slider)	1.321–1.427(calculated from the ethanol solutions)

"–" Indefinite.

baseline has been used to calculate the lowest point of SPR curves [30]. The relationship between different concentrations of ethanol solution and SPR positions has been established and the relationship between the position of the laser line generator and changes of the effective incident angle from the scanning configuration has been analyzed in formula. In our work, the sensing response of this SPR biosensing platform to the bulk refractive index was calibrated using various concentrations of ethanol solution of 5%, 10%, 15%, 20% and 25% in volumetric factions. As a result, this SPR sensing platform was able to detect the change in the refractive index of the ethanol solution with a high linearity and sensitivity at the correlation coefficient of 0.9842 and the sensitivity of 845.60 (RU/Volume fractions). The results obtained from a series of tests confirmed the practicality of this SPR biosensing platform for the detection of a tiny change in refractive index, which can be produced by a variety of bioanalytes. In order to determine the feasibility and optimize the structure of this SPR biosensing platform for bio-molecular interactions in practice, there are still some problems, such as uniform reciprocating motion of the laser line generator, the image shadow and the uncertainty of the area CCD array. All of the above need to be further solved in the future.

Acknowledgments

This research project was financially supported by Henan province joint funding program, Grant no. U1304305 of the National Natural Science Foundation of China, the independent innovation program of State Key Laboratory of Wheat and Maize Crop Science (No. SKL2014ZH-06), Science and Technology Cooperation Project of Henan Province (No.132106000073) and Collaborative Innovation Center of Biomass Energy, Henan Province.

References

[1] Xue TY, Cui XQ, Guan WM, Wang Q, Liu C, Wang H, et al. Surface plasmon resonance technique for directly probing the interaction of DNA and graphene oxide and ultra-sensitive biosensing. Biosens Bioelectron 2014;58:374–9.
[2] Piliarik M, Vala M, Tichy I, Homola J. Compact and low-cost biosensor based on novel approach to spectroscopy of surface plasmons. Biosens Bioelectron 2009;24:3430–5.
[3] Becsi B, Kiss A, Erdodi F. Interaction of protein phosphatase inhibitors with membrane lipids assessed by surface plasmon resonance based binding technique. Chem Phys Lipids 2014;183:68–76.
[4] Sandblad P, Arnell R, Samuelsson J, Fornstedt T. Approach for reliable evaluation of drug proteins interactions using surface plasmon resonance technology. Anal Chem 2009;81:3551–9.
[5] Martinez-Lopez G, Luna-Moreno D, Monzon-Hernandez D, Valdivia-Hernandez R. Optical method to differentiate tequilas based on angular modulation surface plasmon resonance. Opt Lasers Eng 2011;49:675–9.
[6] Ermini ML, Mariani S, Scarano S, Minunni M. Bioanalytical approaches for the detection of single nucleotide polymorphisms by surface plasmon resonance biosensors. Biosens Bioelectron 2014;61:28–37.
[7] Jiang ZX, Qin Y, Peng Z, Chen S, Chen S, Deng C, et al. The simultaneous detection of free and total prostate antigen in serum samples with high sensitivity and specificity by using the dual-channel surface plasmon resonance. Biosens Bioelectron 2014;62:268–73.
[8] Ashley J, Li SFY. An aptamer based surface plasmon resonance biosensor for the detection of bovine catalase in milk. Biosens Bioelectron 2013;48:126–31.
[9] Homola J, Ctyroky J, Skalsky M, Hradilova J, Kolarova P. A surface plasmon resonance based integrated optical sensor. Sens Actuators B Chem 1997;39:286–90.
[10] Zhang DC, Yan YR, Li Q, Yu T, Cheng W, Wang L, et al. Label-free and high-sensitive detection of Salmonella using a surface plasmon resonance DNA-based biosensor. J Biotechnol 2012;160:123–8.
[11] Baer DR, Engelhard MH. XPS analysis of nanostructured materials and biological surfaces. J Electron Spectrosc 2010;178:415–32.
[12] Baer DR, Lea AS, Geller JD, Hammond JS, Kover L, Powell CJ, et al. Approaches to analyzing insulators with Auger electron spectroscopy: update and overview. J Electron Spectrosc 2010;76:80–94.
[13] Fleming Y, Wirtz T, Gysin U, Glatzel T, Wegmannb U, Meyer E. Three dimensional imaging using secondary ion mass spectrometry and atomic force microscopy. Appl Surf Sci 2011;258:1322–7.
[14] Gonzalez FR. Application of capillary gas chromatography to studies on solvation thermodynamics. J Chromatogr A 2004;1037:233–53.
[15] Kirkland JJ, DeStefano JJ. The art and science of forming packed analytical high-performance liquid chromatography columns. J Chromatogr A 2006;1126:50–7.
[16] Makas AL, Troshkov ML. Field gas chromatography–mass spectrometry for fast analysis. J Chromatogr B 2004;800:55–61.
[17] Aizawa H, Tozuka M, Kurosawa S, Kobayashi K, Reddy SM, Higuchi M. Surface plasmon resonance-based trace detection of small molecules by competitive and signal enhancement immunoreaction. Anal Chim Acta 2007;591:191–4.
[18] Song FY, Zhou FM, Wang J, Tao N, Lin J, Vellanoweth RL, et al. Detection of oligonucleotide hybridization at femtomolar level and sequence-specific gene analysis of the Arabidopsis thaliana leaf extract with an ultrasensitive surface plasmon resonance spectrometer. Nucleic Acids Res 2002;30:e72.
[19] Buhl A, Page S, Heegaard NHH, von Landenberg P, Luppa PB. Optical biosensor-based characterization of anti-double-stranded DNA monoclonal antibodies as possible new standards for laboratory tests. Biosens Bioelectron 2009;25:198–203.
[20] Vikinge TP, Hansson KM, Sandstrom P, Liedberg Bo, Lindahl TL, Lundström I, et al. Comparison of surface plasmon resonance and quartz crystal microbalance in the study of whole blood and plasma coagulation. Biosens Bioelectron 2000;15:605–13.
[21] Spackova B, Piliarik M, Kvasnicka P, Themistos C, Rajarajan M, Homola J. Novel concept of multi-channel fiber optic surface plasmon resonance sensor. Sens Actuators B Chem 2009;139:199–203.
[22] Abbas A, Linman MJ, Cheng Q. New trends in instrumental design for surface plasmon resonance-based biosensors. Biosens Bioelectron 2011;26:1815–24.
[23] Jang D, Lim D, Chae GH, Yoo J. A novel algorithm based on the coefficient of determination of linear regression fitting to automatically find the optimum angle for miniaturized surface plasmon resonance measurement. Sens Actuators B 2014;199:488–92.
[24] Kima SJ, Gobi KV, Iwasakac H, Tanakad H, Miura N. Novel miniature SPR immunosensor equipped with all-in-one multi-microchannel sensor chip for detecting low-molecular-weight analytes. Biosens Bioelectron 2007;23:701–7.
[25] Akihide H, Toshihiko I, Yoshio A, Masahiro S, Nobuaki S, Yasukazu A, et al. Development of palm-sized differential plasmon resonance meter based on concept of Sprode. Sens Actuators B 2005;108:893–8.
[26] Akihiro S, Jun K, Yoshikazu M, Showko S, Kazuyasu S. Development of novel optical waveguide surface plasmon resonance (SPR) sensor with dual light emitting diodes. Sens Actuators B 2005;106:383–7.
[27] Chan BL, Jutamulia S. SPR prism sensor using laser line generator. Proc. SPIE 2012;8234:82341P-1.
[28] Hu JD, Li W, Wang TT, Lin Z, Jiang M, Hu F, et al. Development of a label-free and innovative approach based on surface plasmon resonance biosensor for on-site detection of infectious bursal disease virus (IBDV). Biosens Bioelectron 2012;31:475–9.
[29] Zhan SY, Wang XP, Luo ZF, Zhou H, Chen H, Liu Y. Study on design and application of fully automatic miniature surface plasmon resonance concentration analyzer. Sens Actuators B Chem 2011;153:427–33.
[30] Hu JD, Hu JF, Luo FK, Li G, Jiang Z, Zhang R. Design and validation of a low cost surface plasmon resonance bioanalyzer using microprocessors and a touch-screen monitor. Biosens Bioelectron 2009;24:1974–8.